J. Water Environ. Nanotechnol., 8(3): 285-292 Summer 2023

ORIGINAL RESEARCH PAPER

Effect of Copper doped and Magnesium co-doped $BiFeO_3$ for photocatalytic activity

Rajitha Beerelli, Padma Suvarna*

Department of Physics, Jawaharlal Nehru Technological University Ananthapuramu, Andhra Pradesh, India

Received: 2023-05-31 Accepted: 2023-07-01 Published: 2023-08-10

ABSTRACT

In this current research work, the synthesis of Copper (Cu) doped and Magnesium (Mg) co-doped of $BeFiO_3$ (BFO), i.e $BiFe_{1-x}Cu_xO_3$ (where; X= 0.1, 0.15 and 0.2 wt.%) and $Bi_{1-y}Mg_yFe_{1-x}Cu_xO_3$ (where; Y=0.05, 0.1 and 0.15 wt.%) were prepared by sol-gel method. The obtained samples were analyzed by various characterization techniques including X-ray diffraction (XRD), surface morphology examined by field emission scanning electron microscopy (FE-SEM), and transition electron microscopy (TEM). It was noted that Cu (0.15 wt.%) doped BFO had notable photocatalytic activity for Rhodamine (RhB) dye degradation when exposed to visible light irradiation. In addition to Cu (0.15 wt.%) by adding Mg (0.1 wt.%) as a co-doping, exhibited higher photodegradation than the pure BFO, Cu-doped BFO (0.1and 0.2 wt.%) and Mg co-doped BFO (0.05 and 0.15 wt.%). Here we reported a new driven photocatalyst by doping of Cu and co-doping of Mg into BFO simultaneously. These played a key role in hampering the recombination of electron-hole pairs hence the chance to increase dye degradation performance. These findings could be useful for developing affordable photocatalysts for wastewater purification.

Keywords: BFO; Sol-gel method; Cu-doped; Mg co-doped; Rhodamine dye; Photocatalytic activity.

How to cite this article

Beerelli R., Suvarna P., Effect of Copper doped and Magnesium co-doped $BiFeO_3$ for photocatalytic activity. J. Water Environ. Nanotechnol., 2023; 8(3): 285-292. DOI: 10.22090/jwent.2023.03.007

INTRODUCTION

The potential risks associated with contaminating potable water streams have increased due to population and industrialization. Due to the water pollution issues, researchers have taken the initiative to find solutions for that problem. Every industry that uses color, including those in textiles, printing, dyeing, and paper, releases different types of organic dyes such as methyl orange (MO), methyl blue (MB), and rhodamine B (RhB) and drugs such as tetracycline hydrochloride (TC-HCl) into the freshwater streams, producing wastewaters as a result [1-5]. With the increasing demand for potable water, these organic coloring materials need to be processed and it is essential to find effective techniques for treating wastewater. RhB dye can affect the respiratory tract, skin, and gastrointestinal tract irritations and eye infections, significant toxicity to both human and animal development [4,6-7].

Colored waters can be treated using a variety of physical, chemical, and biological techniques. Numerous studies conducted recently on BFO and proved that it can successfully remove organic pollutants. Since light is the only external energy source required for photocatalysts to function, they are especially crucial for environmental applications like air filtration and water purification [8-14]. The BFO as a photocatalyst has attained great recognition due to its small band gap (2.2 to 2.7 eV), nontoxicity, chemical stability, low cost, and good response to visible-light irradiation [15-19]. Although the quick recombination of electrons and holes in pure BFO is a major problem, causing a decrease in photocatalytic activity. To solve this

* Corresponding Authors Email: *padmajntua@gmail.com*

problem, numerous researchers have concentrated on enhancing this photocatalytic activity by doping various transition and rare-earth metals like Cu, Al, Mg and Gd, Ce, Sr, etc. ions [19-22]. Doping with these metal ions to photocatalyst surfaces has been used to increase the lifetime of charge carriers and act as electron traps to prevent the recombination of photoinduced charge carriers. Various methods including the co-precipitation, hydrothermal process, and auto-combustion method have been used to synthesize this ferrite. However, some works have been done on this ferrite such as Samran, B. et.al. The proper Cu concentration in Cu-$BiFeO_3$ was found to be 1.0 mol%, which showed the highest photocatalytic activity for degrading MO aqueous solution under visible light irradiation [2]. Mukesh K. Mishra et.al. The optical properties conveyed that Mg-doped BFO had a comparatively narrow optical energy band gap as compared to that of pure BFO [23]. Our studies show that so far both Cu and Mg-doped BFO by the sol-gel method has been not fabricated.

In this study, pure BFO, Cu-doped, and Mg co-doped BFO were synthesized by sol-gel method with different copper (0.1, 0.15 & 0.2 wt.%) and Magnesium (0.05, 0.1 & 0.15 wt.%). The photocatalytic activities of all samples were examined by the photodegradation of Rhodamine B dye solution under visible light irradiation [24].

EXPERIMENTAL

The samples with the composition of pure $BiFeO_3$, $BiFe_{1-x}Cu_xO_3$, and $Bi_{1-y}Mg_yFe_{1-x}Cu_xO_3$ were synthesized by the sol-gel method.

Preparation of Pure $BiFeO_3$

First, 50 mL of distilled water was used to dissolve 1.91 g of Iron (III) nitrate nano hydrate $Fe(NO_3)_3.9H_2O$ (Analytical-grade) with simultaneous stirring. The pH of the solution was brought to 1 before the addition of bismuth (III) nitrate pentahydrate by adding 10 mL of nitric acid (HNO_3, 65%). Following the addition of 2.42 g of bismuth (III) nitrate pentahydrate $Bi(NO_3)_3.5H_2O$ (Analytical-grade) to the solution, the mixture was continually stirred until a clear solution had formed. As a chelating agent, 25 mL of tartaric acid (M =1) was added drop by drop to the solution. The production of the gel took place after heating the light yellowish transparent solution at 90°C for an hour while stirring continuously then, to facilitate solvent evaporation and powder formation, the temperature was raised to 180°C (or more). The dried powder was calcinated at a temperature of 600°C for three hours, fine brown color was produced and it is labeled as BFO.

Preparation of Cu-Doped $BiFeO_3$

In a similar method to prepare $BiFe_{1-x}Cu_xO_3$, the stoichiometric amount of copper nitrate trihydrate $Cu(NO_3)_3.3H_2O$, with different wt.% (X=0.1, 0.15, and 0.2) added to iron (III) nitrate nano hydrate $Fe(NO_3)_3.9H_2O$, after that the resultant solutions were added to bismuth (III) nitrate pentahydrate $Bi(NO_3)_3.5H_2O$ with continuous stirring till the formation of powder. These prepared samples are labeled as BFC-0.1, BFC-0.15, and BFC-0.2.

Preparation of Mg co-doped $BiFeO_3$

$Bi_{1-y}Mg_yFe_{1-x}Cu_xO_3$ synthesized for the condition BFC-0.15 i.e. to prepare this, magnesium nitrate hexahydrate $Mg(NO_3)_3.6H_2O$ with different wt.% (y=0.05, 0.1 & 0.15) added to iron (III) nitrate nano hydrate $Fe(NO_3)_3.9H_2O$ and copper nitrate trihydrate $Cu(NO_3)_3.3H_2O$ for the wt.%(X= 0.15) added to bismuth (III) nitrate pentahydrate $Bi(NO_3)_3.5H_2O$. Then these two solutions were mixed and stirred continuously until the product was developed. These are labeled as BFMC-0.05, BFMC-0.1, and BFMC-0.15.

CHARACTERIZATION

The synthesized samples were characterized by X-ray diffraction (XRD; Model: Bruker D8 advance), surface morphology examined by field emission scanning electron microscopy (FE-SEM; Model: JEOL 7600) and transition electron microscopy (TEM; Model: JEOLJEM-200X).

RESULTS AND DISCUSSION:

Structural analysis

The XRD patterns of pure BFO, BFC-0.1, BFC-0.15, BFC-0.2, BFMC-0.05, BFMC-0.1 and BFMC-0.15 are shown in Fig. 1.The pure BFO, the peaks were indexed as $2\theta = 22.4^o$, 31.8^o, 32.0^o, 39.5^o, 45.7^o, 51.7^o, 56.4^o, 67.1^o, 71.8^o, 76.0^o. The corresponding plans are (012), (104), (110), (202), (024), (122), (214), (220), (036), and (134) shown in Fig. 1(a) respectively. The sample can be indexed in a single BFO phase for an angle from $2\theta = 20^o$ to 80^o, which is well matched with JCPDS card No. 86-1518 [25] and is hexagonal with the R3c space group. However, a small trace of impurity phase belonging to $Bi_{25}Fe_{40}$ appears for all the doped samples, the

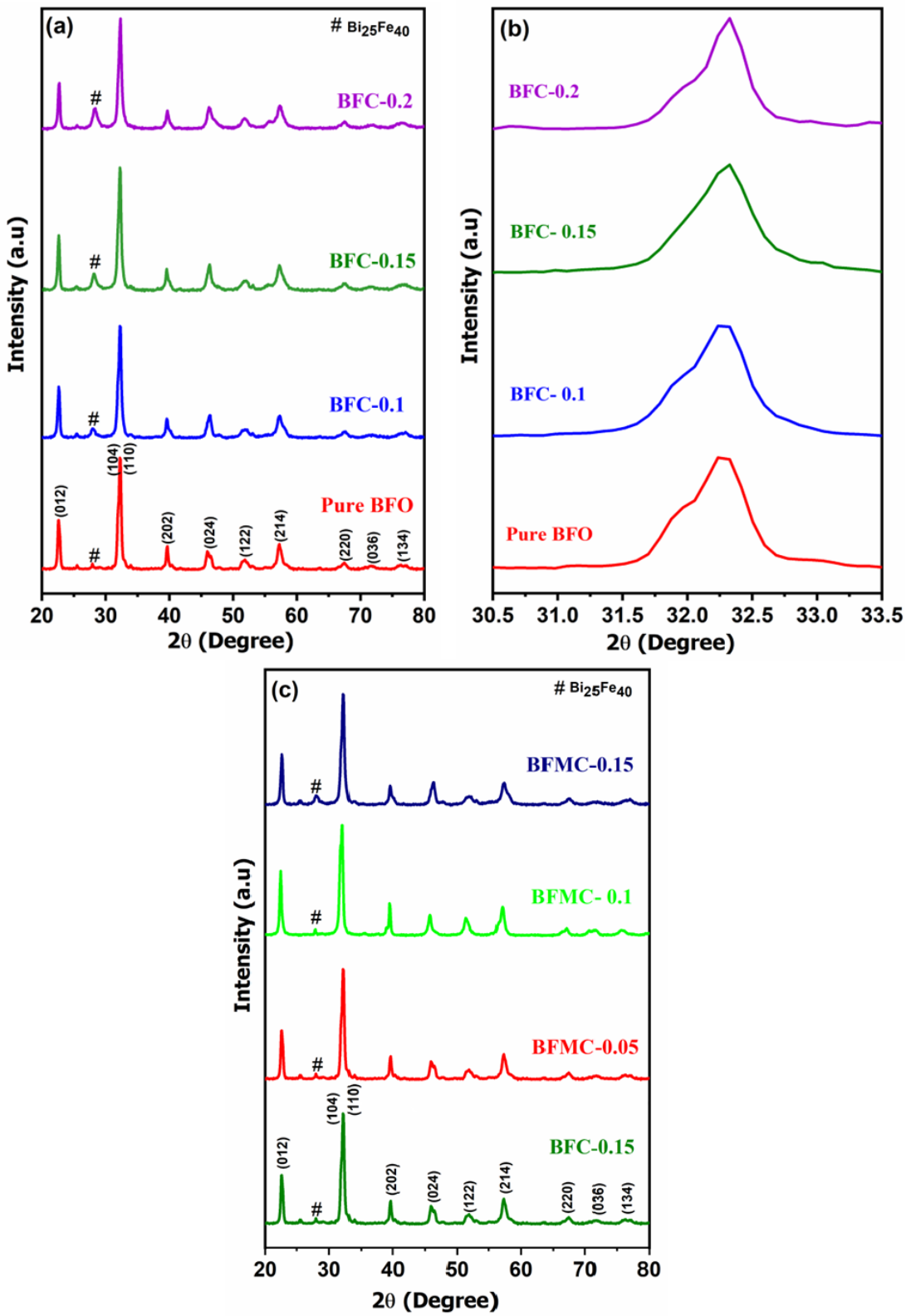

Fig. 1. XRD patterns of (a). Pure BFO and Cu-doped BFO with wt.% 0.1, 0.15, and 0.2 (BFC-0.1, BFC-0.15, and BFC-0.2) BFO (b). The enlarged XRD patterns at 2θ = 30° to 33°, (C). Cu-0.1 wt.% doped BFO (BFC-0.15) and Mg co-doped with wt.% 0.05, 0.1, and 0.15 (BFMC-0.05, BFMC-0.1, and BFMC-0.15).

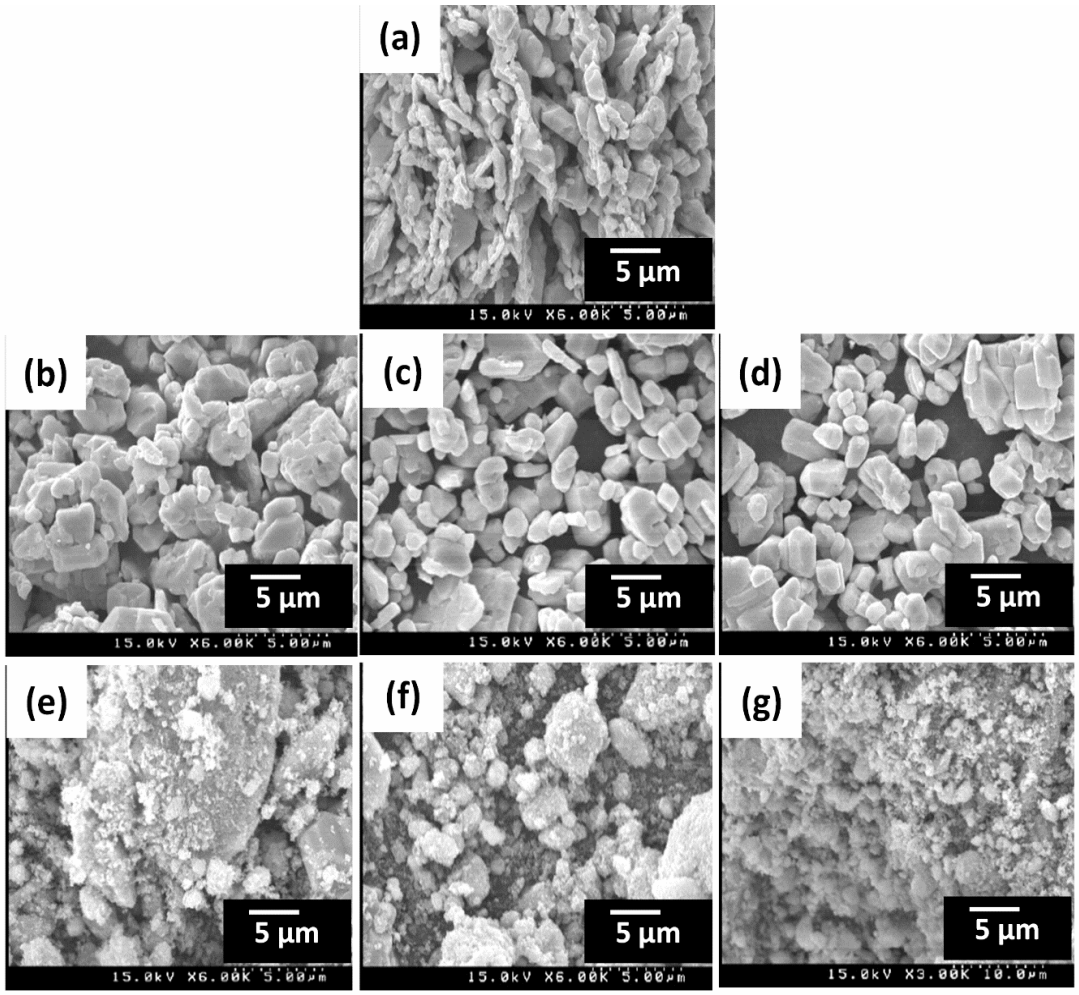

Fig. 2. Filed emission scanning electron microscopy images: (a) pure BFO, (b-d) Cu-doped BFO with wt.% 0.1, 0.15, and 0.2 (BFC-0.1, BFC-0.15, and BFC-0.2), (e-g) Mg co-doped with wt.% 0.05, 0.1, and 0.15 (BFMC-0.05, BFMC-0.1, and BFMC-0.15).

phase shows up 2θ = 29.7°. For the doped samples BDC-0.1, BFC-0.15, and BFC-0.2, when Cu doped with different wt.% in BFO, we enlarge the XRD peaks at 2θ = 32.2° of the sample, the results show that the position of the rhombohedral (110) plane, slightly shift towards a higher angle direction, as shown in Fig. 1(b). Further, by considering the BFC-0.15 constant, the Mg Co-doped with different wt.% such as BFMC-0.05, BFMC-0.1, and BFMC-0.15 in Bi_{1-y} Mg_y $Fe_{0.85}$ $Cu_{0.15}$ O_3, exhibits similar XRD patterns to the pure BFO, without any extra peaks, due to the ion radius of Mg^{2+}(0.71A°) being significantly less than that of Bi^{3+}(1.30A°) [26] as shown in Fig. 1(c). After Mg Co-doped, which is indicating a successful transformation of the rhombohedral crystal structure to a distorted one as well as the increased Co-doped content, the structure transformed from the rhombohedral to the tetragonal structure.

Surface analysis

The surface morphology of pure BFO, Cu-doped, and Mg co-doped BFO samples were analyzed using the field emission scanning electron microscopy (FE-SEM) technique, as displayed in Fig. 2. The FE-SEM image of pure BFO is an irregular structure as shown in Fig. 2 (a). The Cu-doped with different wt.% added into BFO it is observed that a cubic structure is formed. The resultant FE-SEM images were displayed in Fig.. 2(b-d). The morphological and dimensional changes in Cu-doped BFO samples strongly depend on the Cu wt.%. However, after the addition of Mg co-doped with various wt.%

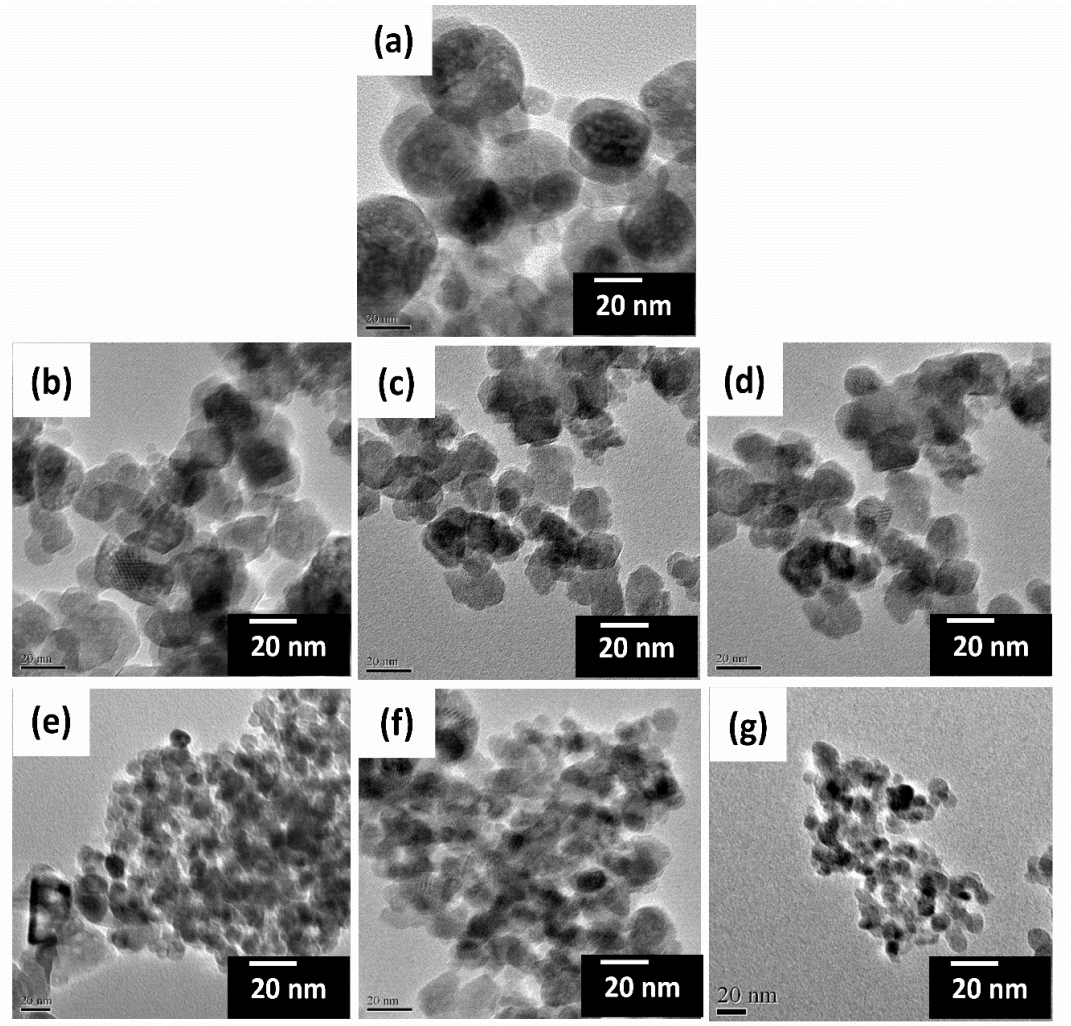

Fig. 3. Transmission Electron Microscopy Images: (a). Pure BFO, (b-d). Cu-doped BFO with wt.% 0.1, 0.15, and 0.2 (BFC-0.1, BFC-0.15 and BFC-0.2), (e-g). Mg co-doped with wt.% 0.05, 0.1, and 0.15 (BFMC-0.05, BFMC-0.1, and BFMC-0.15).

in Cu (BFC-0.15), several pores which cause agglomeration and inhomogeneity are formed as shown in Fig. 2. (e-g).

Transmission Electron Microscopy (TEM) images of pure BFO, Cu-doped, and Mg co-doped BFO samples are illustrated in Fig. 3. TEM image Fig. 3(a) reveals that the pure BFO particles exhibit irregular morphology and are agglomerated with each other, this is due to the result of the high temperature the sample was exposed. Fig. 3(b-d) shows that the Cu-doped (BFC-0.1, BFC-0.15, and BFC-0.2) BFO surface morphology, and Fig. 3(e-g) shows in Mg Co-doped (BFMC-0.05, BFMC-0.1, BFMC-0.15), it was observed the particle size was reduced in case Cu-doped and Mg Co-doped BFO compared to pure.

Photocatalytic activity :

Visible light Irradiation :

Degradation of RhB dye was used to evaluate the photocatalytic activity by the irradiation of visible light of synthesized samples of pure BFO, BFC-0.1, BFC-0.15, and BFC-0.2 and BFMC-0.05, BFMC-0.1, and BFMC-0.15 are present in Fig. 4. In all the below cases first, the prepared solution was placed in a dark condition (Absence of light) and stirred for 60 min to reach the equilibrium between the dye solution and the catalyst. 50 mg of pure BFO was added to 100 mL of dye solution and kept under visible light with continuous stirring and the complete degradation was observed after 150 min which showed in Fig. 4 (a). Further, the same procedure was carried out using Cu-doped BFC-0.1, BFC-0.15, and BFC-0.2, and degradation

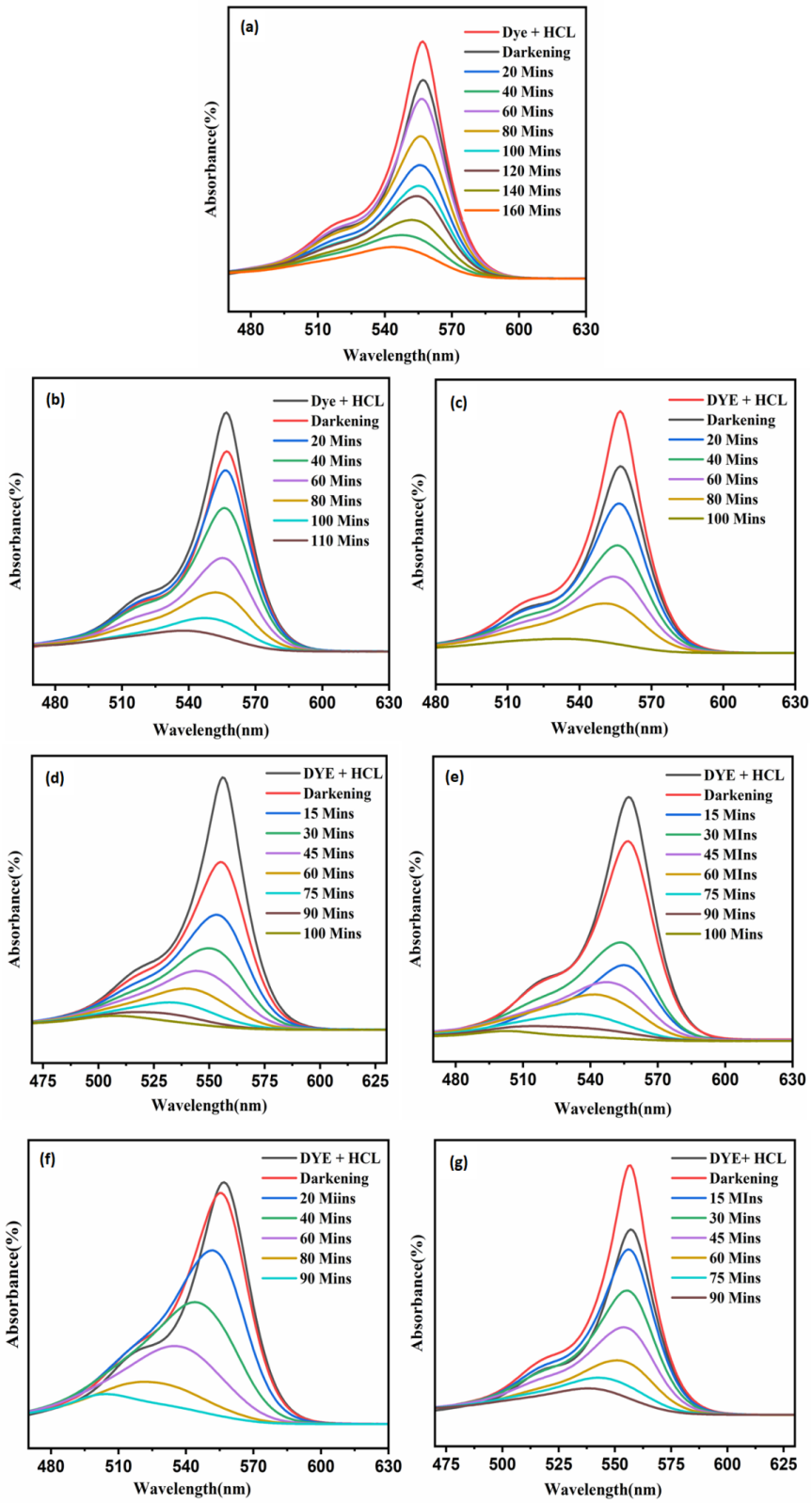

Fig. 4. Photocatalytic degradation of RhB dye: (a) Pure BFO; (b-d) Cu-doped BFO with wt.% 0.1, 0.15, and 0.2 (BFC-0.1, BFC-0.15 and BFC-0.2) (e-g) Mg co-doped with wt.% 0.05, 0.1, and 0.15 (BFMC-0.05, BFMC-0.1 and BFMC-0.15).

was observed at different times as shown in Fig. 4. (b-d). As per the results, the Cu-doped BFC-0.15 sample has given the best removal of RhB dye with less time (100 min) as compared to other samples (BFC-0.1, BFC-0.2). The results strongly suggest choosing Cu-doped BFC-0.15 as an excellent condition for co-doping of Mg as BFMC-0.05, BFMC-0.1, and BFMC-0.15. The Mg co-doped materials showed higher degradation compared to Cu-doped materials as displayed in Fig. 4. (e-g). Finally, degradation was observed in a very short time i.e., only 90 min when Mg with BFMC-0.1 was used as the degradation agent.

Fig. 4 shows the findings from a study on the impact of changing the number of catalysts (Cu-doped and Mg-co doped) on the rate of dye degradation. Up to a specific amount of catalyst, such as for BFC-0.15 and BFMC-0.1, it has been shown that the rate of degradation increases as the amount of catalyst increases [27-30]. The reaction rate becomes almost constant in both scenarios after this point. This phenomenon could be explained by the fact that as catalyst concentration increases, the amount of the catalyst's exposed surface area will also rise. Since the catalyst was entirely covering the bottom of the reaction vessel, the rate of reaction increased as a result. However, if the amount of catalyst is increased over a certain point, just the thickness of the layer (and not the exposed surface area) would grow.

CONCLUSION

In summary, we successfully prepared pure BFO, Cu-doped, and Mg co-doped BFO materials by sol-gel method and characterized by different techniques. X-ray diffraction data shows that all the main peaks were present in all samples. Cu-doped and Mg co-doped in BFO, the structure is transformed from the rhombohedral to the tetragonal structure. The FE-SEM images exhibit the formation of irregular structures observed in pure BFO, the Cu-doped, and Mg co-doped with different wt.% added into BFO it is shown that cubic structure and agglomeration and inhomogeneity are formed. TEM images reveal that irregular morphology was observed in all pure BFO, Cu-doped, and Mg co-doped BFO materials. The Cu doped in BFO was found to be BFC-0.15 was showed the highest photocatalyst activity for degradation of RhB dye aqueous solution under visible light irradiation. The enhanced photocatalytic performance of the Mg co-doped BFMC-0.1 as compared to pure BFO and other Cu-doped BFC-0.1 and BFC-0.2 samples.

ACKNOWLEDGMENT

The author is thankful to the Centre for Nano Science &Technology, University of Engineering Science & Technology, JNTU Hyderabad & University of Hyderabad & Osmania University for providing a lab and instrumentation facility.

CONFLICT OF INTEREST

The authors hereby declare that there is no conflict of interest.

REFERENCES

1. Abdullah IM, Irfan AS, Amin F, et al. (2019) La- and Mn-Codoped Bismuth Ferrite/Ti3C2 MXene Composites for Efficient Photocatalytic Degradation of Congo Red Dye. ACS Omega 4: 8661−8668. https://doi.org/10.1021/acsomega.9b00493
2. Samran B, Krongkitsiri P, Chaiwichian S (2018) Effect of Copper Dopants on Visible-Light-Driven Photocatalytic Activity of BiFeO3 Photocatalysts. Modern Environmental Science and Engineering 4: 234-243.
3. Haruna A, Abdulkadir I, Idris OS (2020) Photocatalytic activity and doping effects of BiFeO3 nanoparticles in model organic dyes. Heliyon 6: 1-8. https://doi.org/10.1016/j.heliyon.2020.e03237
4. Zhao Y, Xu M, Yuanpeng, et al. (2022) Enhanced Photocatalytic Activities for Degradation of Dyes and Drugs by Crystalline Bismuth Ferrite-Modified Graphene Hybrid Aerogel. Crystals 12, 1604. https://doi.org/10.3390/cryst12111604
5. Mohammadzadeh KR, Tayebee R, Ahsani, F (2017) New and highly efficient Ag doped ZnO visible nano photocatalyst for removing of methylene blue. J Mater Sci: Mater Electron, 28(8): 5941-5952. https://doi.org/10.1007/s10854-016-6268-5
6. Al-Gheethi AA, Azhar QM, Kumar SP, et al. (2022) Sustainable approaches for removing Rhodamine B dye using agricultural waste adsorbents: A review. Chemosphere 287: 1-11. https://doi.org/10.1016/j.chemosphere.2021.132080
7. Tayebee R, Mohammadzadeh KR, Audebert P, et al. (2018) A robust UV-visible light-driven SBA-15-PS/phthalhydrazide nanohybrid material with enhanced photocatalytic activity in the photodegradation of methyl orange. Applied Organometallic Chemistry 32(7): e4391. https://doi.org/10.1002/aoc.4391
8. Parvizi E, Tayebee R, Koushki E, et al. (2019) Photocatalytic efficacy of supported tetrazine on MgZnO nanoparticles for the heterogeneous photodegradation of methylene blue and ciprofloxacin. RSC Adv 9(41): 23818-23831. https://doi.org/10.1039/C9RA04702F
9. Jarrahi M, Maleki B, Tayebee R (2019) Photocatalytic efficacy of supported tetrazine on MgZnO nanoparticles for the heterogeneous photodegradation of methylene blue and ciprofloxacin, RSC Adv 9: 23818. https://doi.org/10.1039/C9RA04702F
10. Liu C, Abbaspour S, Rouki M, et al. (2022) Synergistic promotion of the photocatalytic efficacy of CuO

nanoparticles by heteropolyacid-attached melem: Robust photocatalytic efficacy and anticancer performance, Appl Organomet Chem 2022,36: e6878. https://doi.org/10.1002/aoc.6878
11. Li B, Tayebee R, Esmaeili E, et al. (2020) Selective photocatalytic oxidation of aromatic alcohols to aldehydes with air by magnetic WO3ZnO/Fe3O4. In situ photochemical synthesis of 2-substituted benzimidazoles, RSC Adv 10(67): 40725-40738. https://doi.org/10.1039/D0RA08403D
12. Mohammadzadeh KR, Tayebee R, Hedayat S (2017) Phthalhydrazide nanoparticles as new highly reusable organic photocatalyst in the photodegradation of organic and inorganic contaminants, Appl Organometal Chem 32(2): e4033. https://doi.org/10.1002/aoc.4033
13. Chen R, Jalili Z, Tayebee R. (2021) UV-visible light-induced photochemical synthesis of benzimidazoles by coomassie brilliant blue coated on W-ZnO@NH2 nanoparticles, RSC Adv 11(27): 16359-16375. https://doi.org/10.1039/D0RA10843J
14. Jarrahi M, Tayebee R, Maleki B, et al. (2021). One-pot multicomponent green LED photoinduced synthesis of chromeno[4,3-b]chromenes catalyzed by a new nanophotocatalyst histaminium tetrachlorozincate, RSC Adv, 11(32): 19723-19736. https://doi.org/10.1039/D1RA00189B
15. Jia Y, Wu C, Kim D-H, et al. (2018) Nitrogen doped BiFeO3 with enhanced magnetic properties and photo-Fenton catalytic activity for degradation of bisphenol A under visible light. Chemical Engineering Journal 337: 709-721. https://doi.org/10.1016/j.cej.2017.12.137
16. Huo Y, Jin Y, Zhang Y (2010) Citric acid assisted solvothermal synthesis of BiFeO3 microspheres with high visible-light photocatalytic activity. Journal of Molecular Catalysis A: Chemical 331: 15-20. https://doi.org/10.1016/j.molcata.2010.08.009
17. Xian T, Yang H, Dai J F, et al. (2011) Photocatalytic properties of BiFeO3 nanoparticles with different sizes. Materials Letters 65, 1573-1575. https://doi.org/10.1016/j.matlet.2011.02.080
18. Liu Y, Zuo R, Qi S (2013) Controllable preparation of BiFeO3@carbon core/shell nanofibers with enhanced visible photocatalytic activity. Journal of Molecular Catalysis A: Chemical 376: 1-6. https://doi.org/10.1016/j.molcata.2013.04.005
19. Guo R, Fang L, Dong W, et al. (2010) Enhanced Photocatalytic activity and ferromagnetism in Gd doped BiFeO3 nanoparticles. Journal of Physical Chemistry C 144: 21390-21396. https://doi.org/10.1021/jp104660a
20. Di LJ, Yang H, Hu G, et al. (2014) Enhanced photocatalytic activity of BiFeO3 particles by surface decoration with Ag nanoparticles. J Mater Sci: Mater Electron 25: 2463-2469. https://doi.org/10.1007/s10854-014-1896-0
21. Arora M, Kumar M (2014) Electron spin resonance probed enhanced magnetization and optical properties of Sm-doped BiFeO3 nanoparticles. Materials Letters 137: 285-288. https://doi.org/10.1016/j.matlet.2014.08.140
22. Wei Z, Abbaspour S, Tayebee R (2023) Nickel Nanoparticles Originated from Cressa Leaf Extract in the Preparation of a Novel Melem@Ni-HPA Photocatalyst for the Synthesis of Some Chromenes and a Preliminary MTT Assay on the Anticancer Activity of the Nanocomposite, Polycyclic Aromatic Compounds 43:1: 552-571. https://doi.org/10.1080/10406638.2021.2019063
23. Mishra MK, Mahaling RN (2017) Mg doping in BiFeO3: An advantage over pure BiFeO3 having enhanced ferroelectric and optical properties for opto-electronic device applications, Ferroelectrics 520(1): 184-195. https://doi.org/10.1080/00150193.2017.1388764
24. Rajitha B, Rao VK, Suvarna PR (2019) Synthesis of multiferroic BiFeO3 microcrystals for photocatalytic activity and stability performance. Materials Today: Proceedings 26: 126-129. https://doi.org/10.1016/j.matpr.2019.06.325
25. Ghahfarokhi EMS, Helfi K, Shoushtari ZM (2022) Synthesis of the Single-Phase Bismuth Ferrite (BiFeO3) Nanoparticle and Investigation of Their Structural, Magnetic, Optical and Photocatalytic Properties. Advanced Journal of Chemistry-Section A 5: 45-58.
26. Lin D-Y, Chen H-Z, Kao M-C, et al. (2020) Ferroelectric and Electrical Properties Optimization of Mg-doped BiFeO3 Flexible Multiferroic Films. Summetry 12: 1173. https://doi.org/10.3390/sym12071173
27. Shokri A, Mahanpoor K (2016) Removal of Ortho-Toluidine from Industrial Wastewater by UV/TiO2 Process, Journal of Chemical Health Risks 6(3): 213-223.
28. Karimi S, Shokri A (2021) The removal of Hexavalent chromium; (Cr (VI)) by ZnO/LECA as a nano photocatalyst using full factorial experimental design, J. Nanoanalysis 8(3): 167-175.
29. Shokri A (2021) Using NiFe2O4 as a nano photocatalyst for degradation of polyvinyl alcohol in synthetic wastewater, Environmental Challenges 5: 100332. https://doi.org/10.1016/j.envc.2021.100332
30. Shokri A (2020) Using Mn based on lightweight expanded clay aggregate (LECA) as an original catalyst for the removal of NO2 pollutant in aqueous environment, Surfaces and Interfaces 21: 100705 https://doi.org/10.1016/j.surfin.2020.100705